## Metals & corrosion

# The hot deformation behaviour of laser powder bed fusion deposited Al–Si–Cu alloy processed by high-pressure torsion

Ahmed S. J. Al-Zubaydi[1,2,*] , Nong Gao[1] , Jan Dzugan[3] , Pavel Podany[3] ,
Sandeep Sahu[1] , Deepak Kumar[1] , Ying Chen[4], and Philippa A. S. Reed[1]

[1] School of Engineering, Faculty of Engineering and Physical Sciences, University of Southampton, Southampton SO17 1BJ, UK
[2] School of Applied Sciences, University of Technology-Iraq, Baghdad, Iraq
[3] COMTES FHT a.s. Company, Průmyslová 995, 334 41 Dobřany, Czech Republic
[4] School of Materials Science and Engineering, Xiamen University of Technology, Xiamen 361024, China

## ABSTRACT

The tensile properties of an ultrafine-grained Al–9%Si–3%Cu alloy deposited by the laser powder bed fusion process have been investigated in this work. The additively manufactured (AM) alloy was subjected to high-pressure torsion processing at room temperature successfully at different number of turns in HPT and then inspected through hot tensile testing at 298 and 573 K using strain rates ranging from $10^{-1}$ to $10^{-4}$ s$^{-1}$. The processed alloy showed extensive refinement and high dislocation density that was associated with considerable strength at ambient temperature. The as-deposited and processed samples of the alloy exhibited significantly higher tensile strength and elongation under hot deformation conditions compared with their cast counterpart alloys. The room temperature-HPT processing presented ultrafine $\alpha$-Al and well-distributed nanosized eutectic Si particles which significantly improved the tensile behaviour and thermal stability of the processed microstructures. The formation of fibrous structures has enhanced the flow behaviour and cavitation resistance at the elevated testing temperature. The current work indicates the impact of room temperature-HPT processing on the mechanical performance of the controllable AM-deposited alloy to meet industrial needs without further heat treatments or alloying additions.

---

Handling Editor: Sophie Primig.

Address correspondence to E-mail: asaz1f20@soton.ac.uk

## Introduction

Aluminium–silicon alloys are commonly employed in the automobile industry such as engine blocks and cylinder heads [1, 2], due to their good lightweight, castability, good machinability, and recyclability [3, 4]. The Al-Si alloy system normally consists of a eutectic composition of 12% silicon, with hypoeutectic and hypereutectic forms of these alloys containing less and more than 12% silicon, respectively [1, 5]. The mechanical performance of the Al-Si alloys is controlled by the microstructural morphology of α-Al and eutectic Si phases, where the coarse grain size in the cast Al-Si alloys has a detrimental effect on the strength and plasticity [6, 7]. Therefore, microstructural refinement of Al-Si alloys offers a pathway to improve the mechanical properties at ambient and elevated temperatures. Different severe plastic deformation (SPD) processes such as high-pressure torsion (HPT) and equal channel angular pressing (ECAP) have been used to produce ultrafine-grained Al-Si alloys with better reported properties.

HPT has previously been conducted at temperatures of 298 and 445 K on cast Al–7%Si alloy up to 10 turns, which resulted in a finer grain size of 400 nm and a hardness increase from 42HV for the as-cast unprocessed alloy to 75HV when processing at the lowest processing temperature. The enhancement in hardness was imputed to outstanding microstructural refinement of the α-Al and eutectic Si phases achieved at room temperature [8]. HPT was also conducted at room temperature on cast Al–7%Si alloy up to 10 turns which also resulted in substantial microstructural refinement down to 78 and 59 nm for the α-Al and eutectic Si phases, respectively. A hardness increase from 49HV for the as-cast unprocessed alloy to 153HV was observed after HPT with enhanced wear resistance attributed to the extensive microstructural refinement and homogeneous distribution of silicon eutectic particles [9]. Another investigation of HPT processing at room temperature in cast Al–7%Si alloy processed up to 10 turns showed a hardness enhancement up to 185HV and improvement in the corrosion resistance, whereas the initial hardness for the as-cast unprocessed alloy was 71HV. Formation of strain-induced sites during HPT processing has resulted in the development of protective thick oxide films that enhanced the corrosion behaviour of HPT-processed alloy [10].

A rotary-die ECAP of cast Al–11%Si alloy was conducted at 573 K up to 32 passes. A modest increase in tensile elongation of this alloy was seen up to 34% with the increase in number of passes and at a temperature of tensile testing up to 573 K. The heat treatment of this alloy resulted in a noticeable increase in the tensile strength and elongation owing to submicron grain size and the uniform distribution of the silicon eutectic phase particles [11, 12]. It is worth mentioning that the rotary-die ECAP is considered as continuous ECAP processing with an imposed strain for each pass as higher as 15% than in the conventional ECAP. This allows for processing at a higher number of passes at the same processing temperature that will be maintained steadily for the processed sample rather than removal and reheating of the processed samples as in conventional ECAP [11, 13]. It was found that the strength of Al–Si alloys processed by ECAP depends on the processing temperature. The room temperature-ECAP processing of the cast Al–10%Si alloy was not successful without prior heat treatment and extended to only two passes. Instead, ECAP on the alloy was carried out at high temperatures up to 573 K up to four passes. The processed samples at room temperature showed a significant higher strength (in term of hardness measurement) than at elevated temperature [14]. Another investigation was conducted on the ECAP processing of semi-solid Al–7%Si alloy at temperatures of 473–573 K with up to eight passes producing a grain size of 2 μm. The tensile strength and elongation were slightly increased to 350 MPa and 28%, respectively, in comparison with the as-cast Al–7%Si alloy. Higher processing temperature resulted in a lower ductility due to particle coarsening of the silicon eutectic phase [15]. From the studies mentioned above, it can be concluded that the majority of HPT and ECAP processing has been carried out on traditional cast Al–Si alloys.

In recent years, additively manufactured aluminium alloys have shown significant improvement of mechanical properties compared to their cast counterparts. This comes from the capability of manufacturing a controllable microstructure at high levels of purity and precision, through careful process parameter selection, which allows predetermined properties to be achieved that are not possible in casting processes [4, 16–18]. Therefore, a combination of additive manufacturing with severe plastic deformation of aluminium alloys may give

significant performance enhancement associated with controllable ultrafine microstructure. Such a study allows a deeper investigation of how such refined microstructures may be controlled to achieve particular properties.

Reviewing previous work in Al–Si alloys, no investigation to date has been conducted on the tensile behaviour of HPT-processed additively manufactured Al–Si alloys. For the first time, this work presents an investigation of the influence of room temperature-HPT processing on an Al–9%Si–3%Cu alloy additively manufactured by laser powder bed fusion (LPBF) on subsequent tensile properties at ambient and high temperatures. The relationship between grain refinement that occurs in the α-Al matrix and eutectic silicon phase and the tensile strength, elongation to failure, and fracture micromechanisms when these microstructures are tested in tension at 298 and 573 K is analysed and discussed. This study provides comprehensive understanding about the modification induced by HPT processing into an additively manufactured Al–Si alloy which allows improved mechanical performance in this type of alloy.

## Materials and methods

Al–9%Si–3%Cu aluminium alloy was AM-deposited by LPBF in the form of a rod with vertical Z-orientation. The alloy fabrication was achieved under nitrogen atmosphere using a Concept Laser M2 facility using a laser power of 200 W, a scan speed of $1000 \text{ mms}^{-1}$, a hatch spacing of 200 μm, and a layer thickness of 40 μm. The weight composition presented in Table 1 for the alloy under investigation was obtained by energy-dispersive spectroscopy (EDS) using an elemental mapping profile. The alloy rod was cut using a wire discharge machine into disc-shaped samples with diameters and thicknesses of 10 mm and 0.85 mm, respectively, to be placed between the HPT anvils for processing. Processing through HPT was carried out at room temperature through a quasi-constrained mode with 6.0 GPa as applied pressure and at different turns of 1/2, 1, 5,

and 10 at speed of 1 revolution per minute [19]. The sample's thickness after 10 turns was about 0.7 mm.

Mechanical grinding and polishing by SiC papers and 1 μm diamond paste, respectively, were applied to the as-deposited and processed samples. A Keller's reagent was used for chemical etching of these polished samples for 10 s followed by drying using ethanol and compressed air, respectively. The etched as-deposited and processed samples then were investigated using optical microscopy (OM), scanning electron microscopy (SEM). Transmission electron microscopy (TEM) of the processed microstructure was carried out using miniature samples obtained from the edge region of the HPT disc as displayed in Fig. 1. These samples were in the form of small discs with 100 μm thickness and 3 mm in diameter, respectively. Electropolishing of these samples was conducted using a solution of 30% $HNO_3$ in $CH_3OH$ in a twin–jet electropolisher at − 30 °C and 20 V. X-ray diffraction (XRD) analysis of the as-deposited and processed samples was achieved using Kα-Cu radiation source from 30–90°, where the XRD patterns were fitted by the Rietveld refinement method. These data were used to measure the density of dislocations ($\rho$) via the relation: $\rho = 2(3\varepsilon)^{1/2}/Db$, where $\varepsilon$, $D$, and $\boldsymbol{b}$ are the microstrain, crystallite size, and Burgers vector of the aluminium, respectively, (0.286 nm [20]). Vickers microhardness was conducted over the HPT disc's diameter as illustrated in Fig. 1, using a 100 gf as force load for 15 s, where each point ( × ) represents an average of four readings separated by a distance of
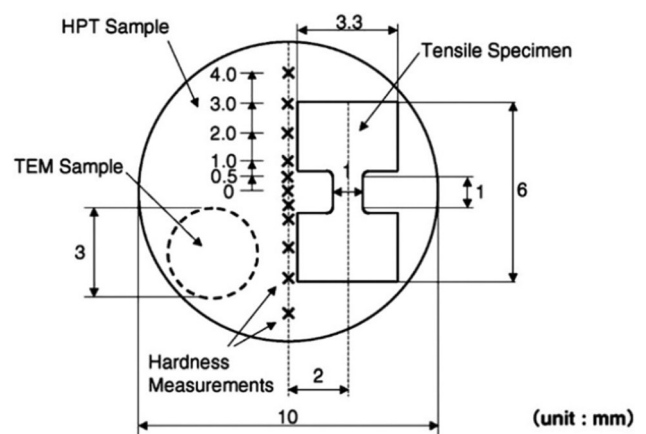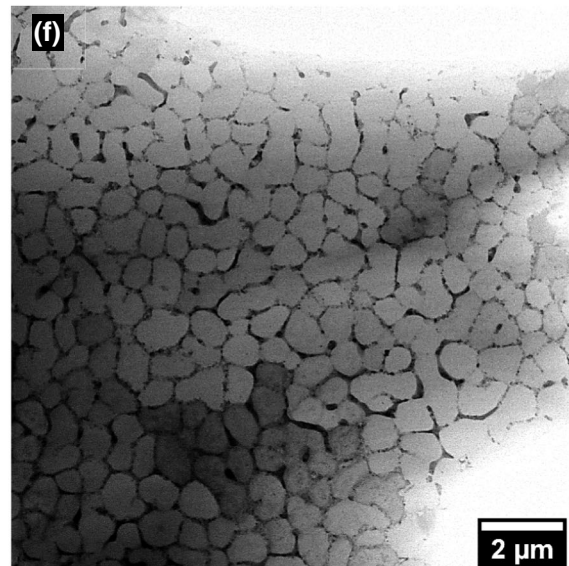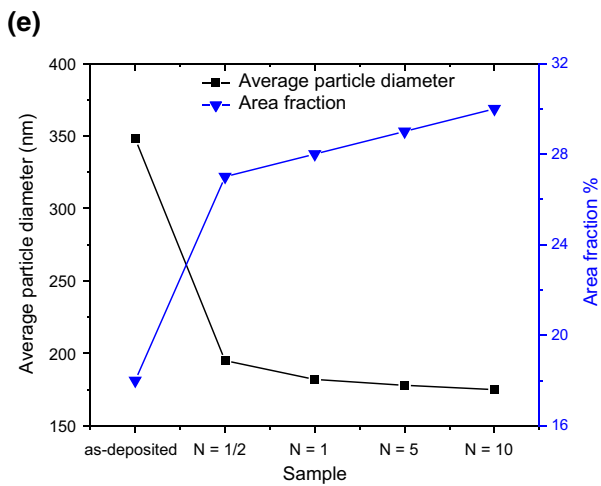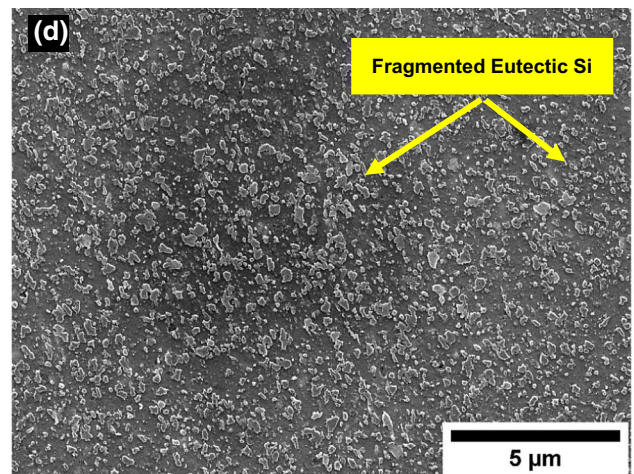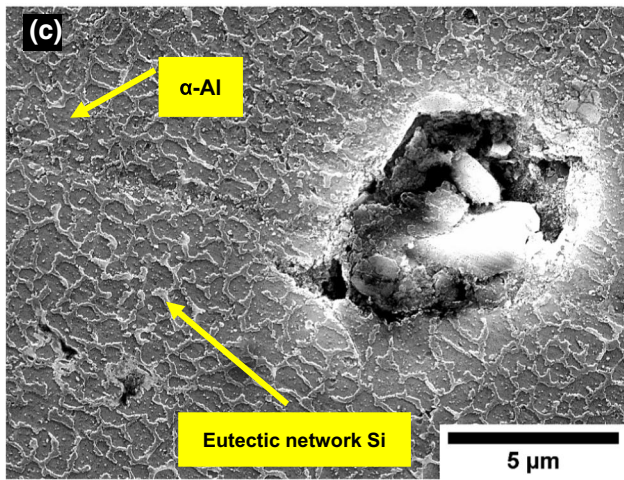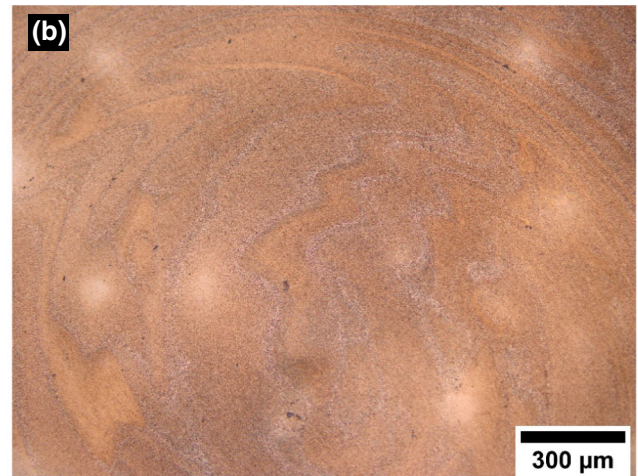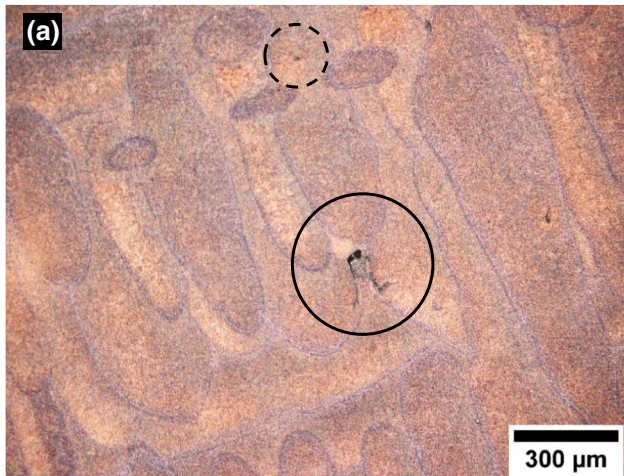


**Figure 1** An illustration on the HPT disc presenting the locations of cut samples for the tensile and TEM investigation as well as the hardness measurement [20, 21].

**Table 1** Chemical analysis (%wt) of the investigated AM-deposited Al–9%Si–3%Cu alloy

| Al | Si | Cu | Fe | Mg |
| --- | --- | --- | --- | --- |
| Bal | 9.1 | 3.2 | 0.5 | 0.3 |

◀**Figure 2** Microstructural observations over the HPT discs showing **a** as-deposited sample and **b** 10 turns HPT-processed sample as seen by OM, **c** as-deposited sample, **d** 10 turns HPT-processed sample as seen by SEM, **e** the average particle diameter and area fraction percentage of the fragmented eutectic silicon phase in the HPT-processed samples as well as in the as-deposited sample, **f–h** TEM observation of the as-deposited alloy, 1/2 and 10 turns HPT-processed samples at the disc periphery, and **i** EDS analysis of the 10 turns HPT-processed sample in (**h**).

150 µm [21]. SEM micrographs and ImageJ analysis software were employed to calculated the average particle diameter and area fraction distribution of the eutectic silicon phase particles in the HPT-processed samples as well as in as-deposited sample [22]. Field areas on each etched sample were selected and transformed into carefully thresholded relative grey level areas to be measured using Image J.

The tensile samples were prepared by cutting micro-tensile samples as reported earlier [23–27] with dimensions of $(1.0 \times 0.9 \times 0.6)$ mm$^3$ as exhibited schematically in Fig. 1. Two tensile samples were taken from each HPT disc where all tensile samples were cut in off-centre positions to exclude the structural heterogeneity that originated in the central areas of samples after HPT. The tensile test was conducted in an air atmosphere using rates of strain starting from $10^{-1}$ to $10^{-4}$ s$^{-1}$ at room temperature (298 K) and
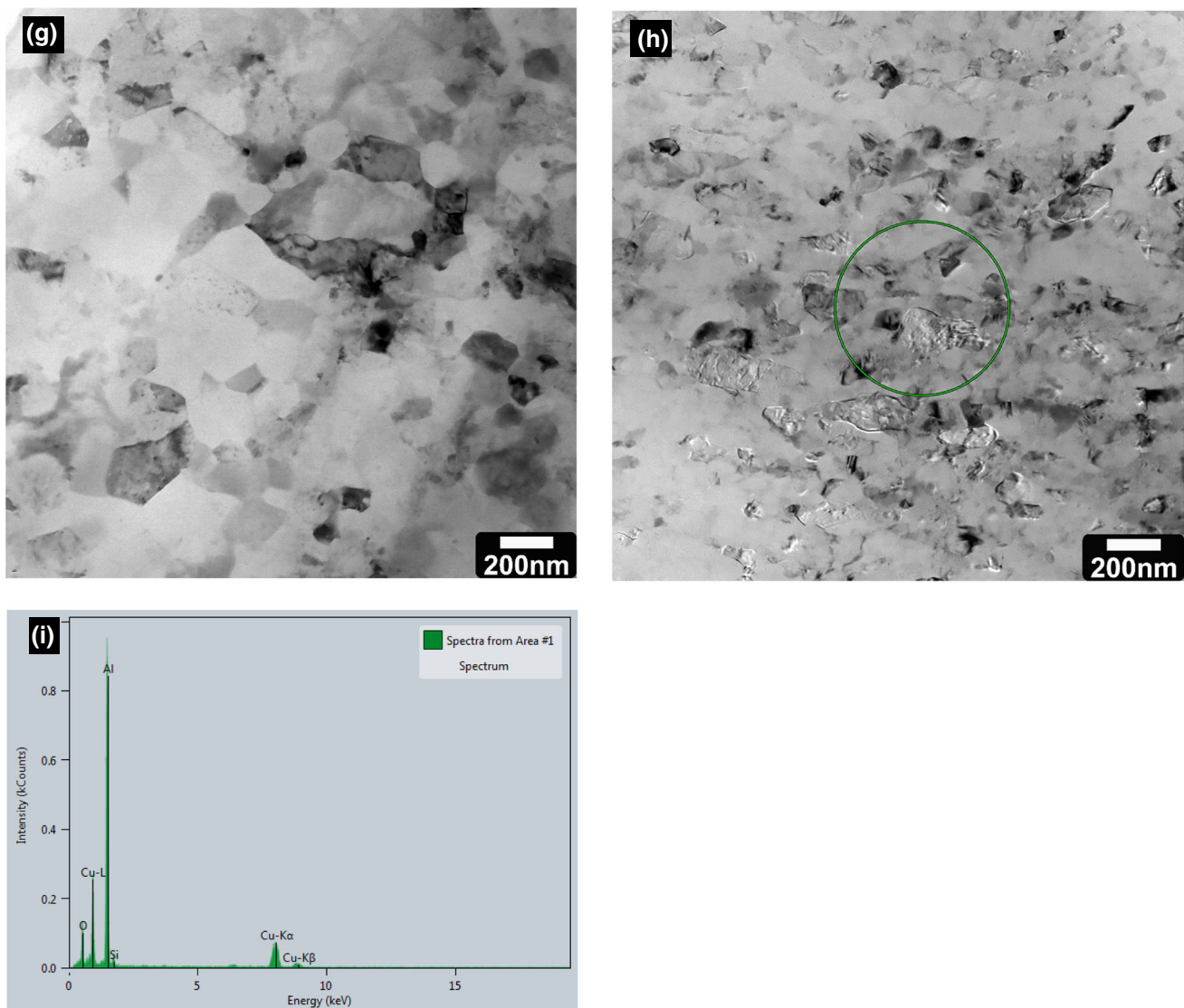
**Figure 2** continued.

at elevated temperature (573 K) for the tensile samples that were obtained from the HPT discs processed for 1/2, 1, 5 and 10 turns, as well as for the as-deposited unprocessed samples. Four tensile samples were tested for each condition to assess scatter. Engineering stress–strain, elongation-strain rate and flow stress–strain rate curves were constructed. The microstructures within the gauge sections of the tensile samples were seen using SEM. The chemical composition of the samples before and after tensile testing were obtained. The fractured tensile samples were reconstructed in representative images by low-magnification OM, where these images present the resultant elongation for each strain rate and testing temperature.

## Results

The microstructures of the AM-deposited Al–9%Si–3%Cu alloy before and after HPT are presented in Fig. 2. Elemental weight fractions of the alloy are shown in Table 1. Using the OM observations, the as-deposited sample over the horizontal disc plane obviously exhibits melt pool structures of different lengths and with an average width of 150 μm. Porosity of process-induced and gas-induced types were also observed in the as-deposited samples as indicated, respectively, by the solid and dashed circles in Fig. 2a.

After HPT processing, these pool structures were seen to gradually disappear in the processed samples up to 10 turns as demonstrated in Fig. 2b, c. The etched as-deposited sample showed a dark phase of α-Al matrix and white eutectic Si in the form of a continuous network as shown in Fig. 2c. Following the HPT, this morphology has altered as observed in Fig. 2d, where the eutectic network has experienced a gradual shearing and fragmentation down to the nanoscale as the number of HPT turns increased up to 10 turns. The measurements of average particle diameter and area fraction of the fragmentation of eutectic silicon phase for both as-deposited and HPT-processed samples are illustrated in Fig. 2e. Initial grain size of the as-deposited alloy as revealed by TEM observation was 1 μm as shown in Fig. 2f. TEM observations of the processed alloy showed a development of fine grains as observed for 1/2 and 10 turns HPT-deformed samples as shown in Fig. 2g–h, where the final grain size has reached about 90 nm.

The chemical composition of elements in the HPT-processed sample for 10 turns is shown in Fig. 2i.

Measurements of the crystallite size via XRD profiles that presented in Fig. 3a, b for the as-deposited and HPT-processed samples showed a significant microstructural refinement from 320 nm in the as-deposited sample to 30 nm in the HPT-processed sample for 10 turns as represented in Fig. 3c. It is expected that the grain size will be 3–4 times the crystallite size in the current processed alloy [20, 28]. A remarkable rise was found in the density of dislocations for the processed samples in proportion with the number of turns as illustrated in Fig. 3c. A considerable dislocation density was stored in the alloy, up to $6.2 \times 10^{14}$ m$^{-2}$ at 10 HPT turns, while the initial dislocation density of the as-deposited alloy was about $1 \times 10^{14}$ m$^{-2}$.

A significant increase in the hardness of HPT-processed alloy was observed with a higher number of turns compared to the as-deposited alloy, as illustrated in Fig. 4. Initially, the as-deposited sample showed an average hardness of 120HV. Following the HPT processing, the alloy showed a faster rate in hardness increase at the peripheries compared to the centres of the disc-shaped samples in the initial stage of HPT processing. Later, a relative saturation in achieved hardness at both centre and periphery regions was noticed at higher numbers of HPT turns, where the average achieved value of the hardness was about 240HV after 10 HPT turns.

A typical engineering stress–strain behaviour of the as-deposited and processed additive manufactured Al–Si–Cu samples is shown in Figs. 5 and 6, for samples processed by 10 turns, then tested to fracture through tensile testing at 298 K and 573 K at different strain rates starting from $10^{-1}$ to $10^{-4}$ s$^{-1}$. The testing temperature of 573 K corresponds 0.65 $T_m$, where the melting point of the Al–9%Si–3%Cu alloy is 873 K (600 °C) [1].

The tensile curves showed an increase in the elongation to fracture with higher testing temperature, increasing number of HPT turns and at slower strain rates. The strain hardening behaviour of the deformed samples increased with increasing number of HPT turns and increasing strain rate in comparison with the as-deposited samples. The HPT-processed samples tensile tested at 573 K showed lower values of ultimate-tensile stresses compared to the as-deposited samples as shown in Figs. 5 and 6b, especially at slower strain rates.
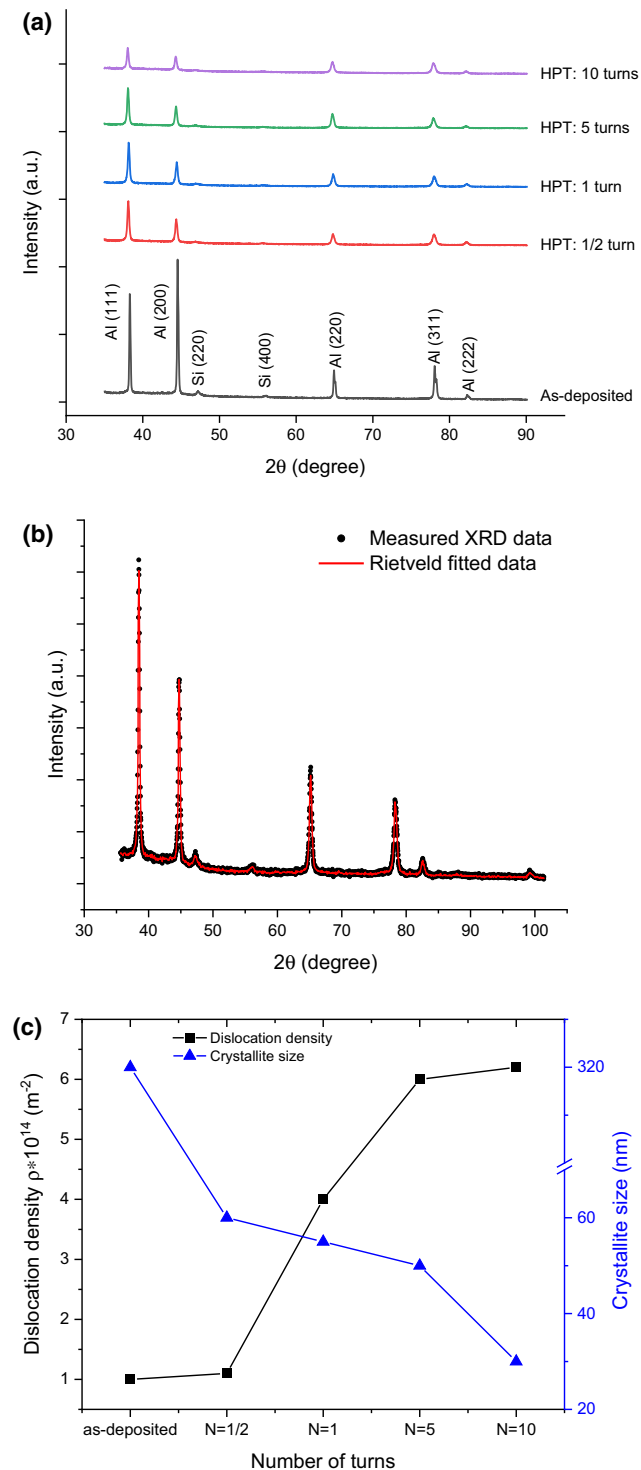
**Figure 3** **a** XRD patterns for the as-deposited and HPT-processed samples, **b** XRD measured profile and Rietveld fitted data of the alloy as represented in black scattered dots and solid colourful line, respectively, and **c** Development in the dislocation density and XRD-crystallite size in the as-deposited and HPT-processed disc-shaped samples.
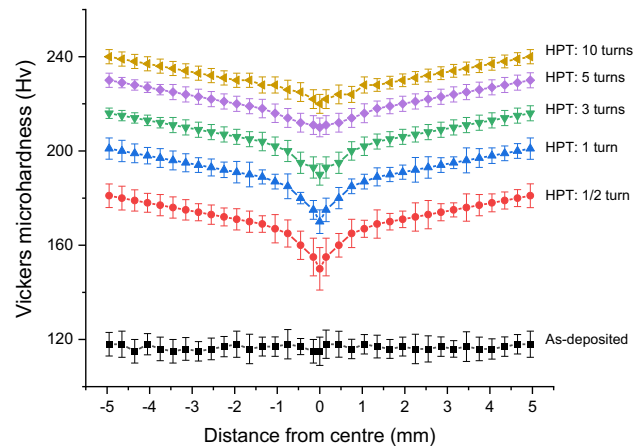


**Figure 4** The distribution of Vickers microhardness along the diameters of as-deposited and HPT-processed disc-shaped samples.

The percentage elongations of all processed samples showed an increase with an increase in the number of turns, increase in testing temperature and decrease in strain rate compared to the as-deposited samples. The percentage elongations for the processed samples showed an improvement at high testing temperature compared to the as-deposited sample as shown in Figs. 7 and 8, where the HPT-deformed sample for 10 turns showed the highest elongation of 220% at $10^{-4}$ s$^{-1}$ strain rate and at a test temperature of 573 K.

The values of strain rate sensitivity were calculated in the as-deposited and processed samples after 10 turns as represented in Fig. 9. These values were extracted from the slopes of the log–log plots in Fig. 9 for all the strain rate ranges studied in this investigation at 573 K. This sensitivity for the deformed samples was higher than that seen in the as-deposited samples for all strain rates. Its value showed a relative increase from $10^{-2}$ to $10^{-3}$ s$^{-1}$ that was associated with lower flow stresses and significant elongations in the case of the processed sample after 10 turns in HPT.

The microstructures over the gauge lengths of the fractured tensile samples were investigated by SEM as shown in Figs. 10 and 11. These microstructures belonged to tensile samples that were cut and tested from as-deposited samples and HPT-processed for 10 turns at 573 K at all strain rates as represented in Fig. 7. The processed sample after 10 turns showed substantial microstructural stability after the tensile test with an average grain size of 5 μm ± 0.3 μm for
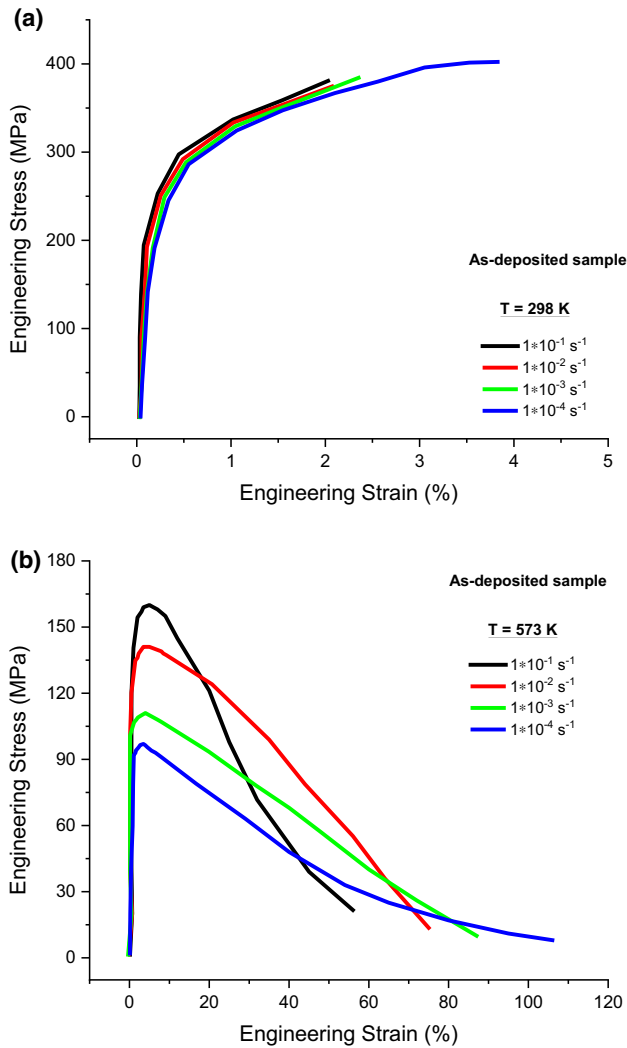
**Figure 5** The engineering stress–strain behaviour of the as-deposited sample that inspected through the tensile test at **a** 298 K, and **b** 573 K at various rates of strain.

**Figure 6** The engineering stress–strain behaviour of the HPT-processed sample for 10 turns that inspected through the tensile test at **a** 298 K, and **b** 573 K at various rates of strain.

the all strain rates studied, whereas the as-deposited samples showed average grain sizes of 10 μm ± 0.4 μm after the tensile test associated with significant cavitation among the grain boundaries.

The grain morphology remained equiaxed after testing for the as-deposited and developed fibrous structures as in the processed samples as shown in Figs. 10 and 11. These fibrous structures were seen to connect the grains in the processed sample during testing at slower strain rates. The chemical analysis of these fibrous structures obtained by the EDS is shown in Fig. 12, where these structures are mainly composed of the alloy matrix composition.
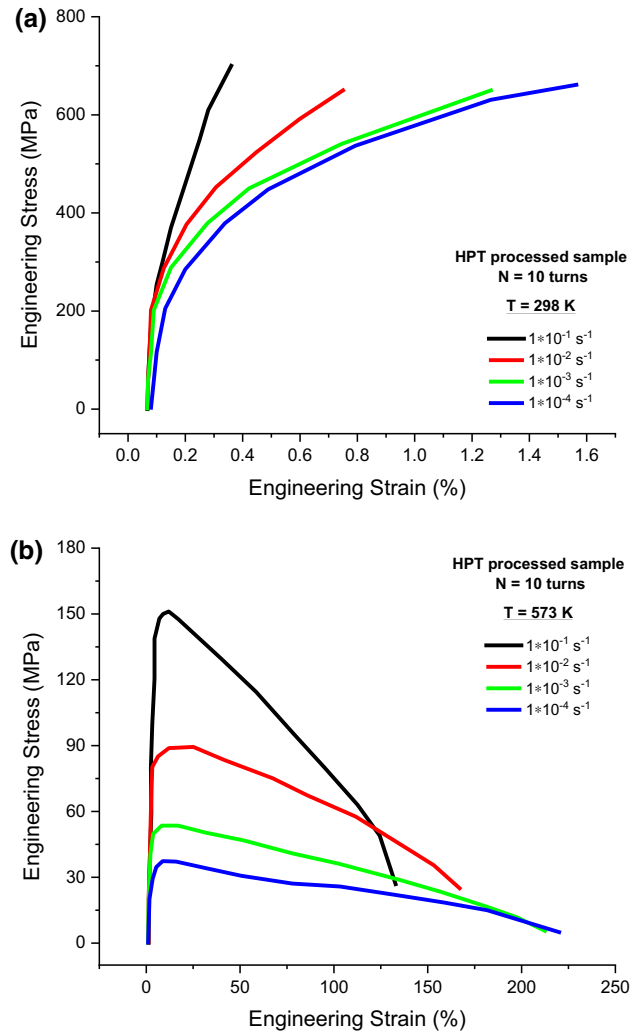
# Discussion

## Microstructural refinement

The AM-deposited Al–9%Si–3%Cu alloy was effectively deformed using room temperature-HPT in this investigation. The achieved microstructural refinement as obtained by grain size and crystallite size measurements were found to be about 90 and 30 nm, respectively, after 10 turns in HPT, which is ascribed to the influence of the processing temperature on the level of achievable microstructural refinement during severe plastic deformation processes. The current processing was done at room temperature so there was no dynamic recovery, recrystallization or even grain growth that would affect the extent of the grain
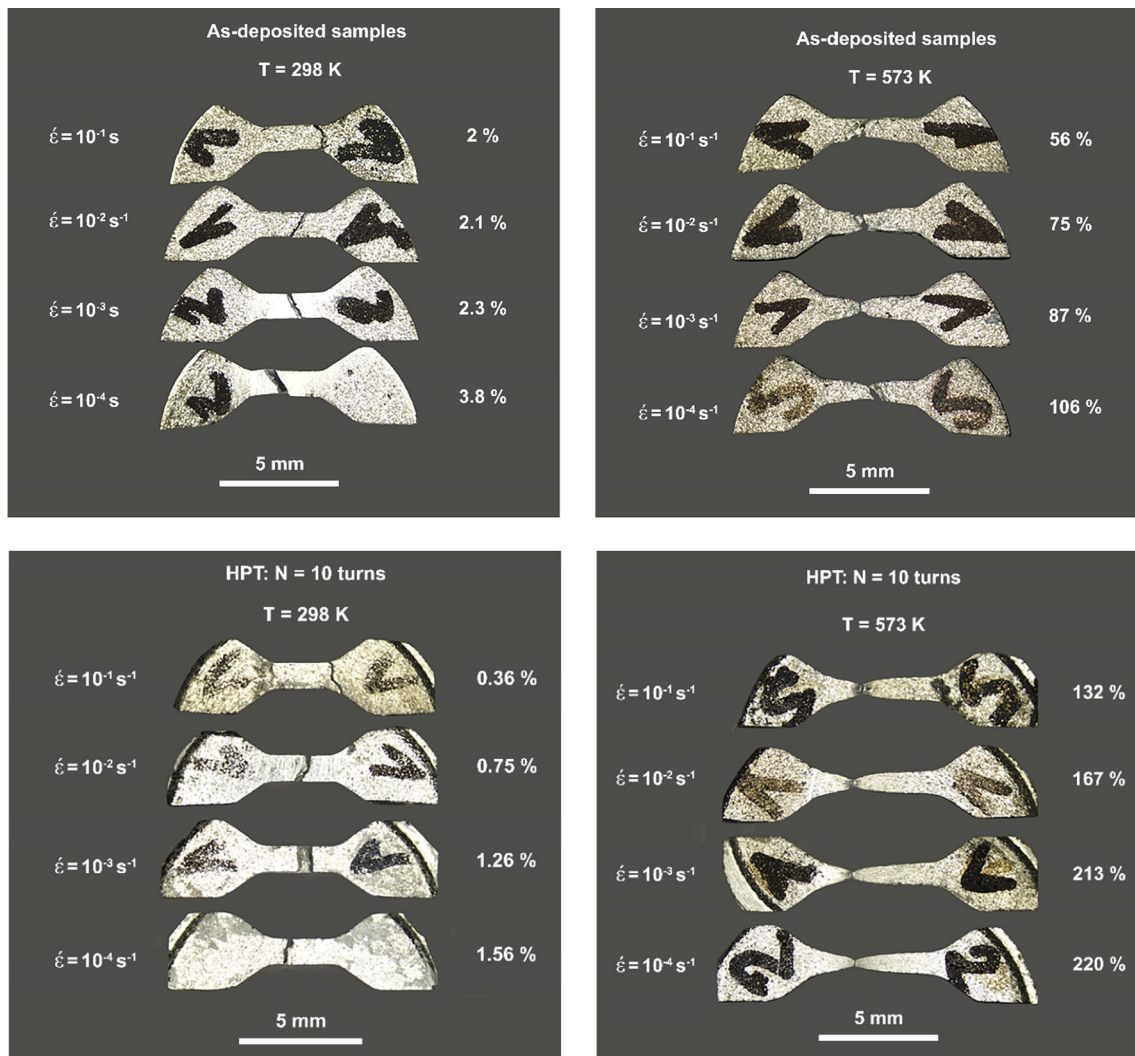
**Figure 7** Appearance of the as-deposited and 10 turns HPT-processed samples that fractured in the tensile testing at 298 K and 573 K and various rates of strain.

refinement with the high levels of imposed deformation during HPT.

The severe plastic deformation imposed was higher after a high number of HPT turns, where the grain size and crystallite size were found to be inversely proportional with the preceding deformation. The HPT imposed strain was translated into significant grain refinement of the AM processed alloy from a size of 1 μm to 90 and 30 nm for grain size and crystallite size, respectively. A considerable dislocation density was stored in the alloy, up to $6.2 \times 10^{14}$ m$^{-2}$, at such levels of imposed strain, while the initial dislocation density of the as-deposited unprocessed alloy was about $1 \times 10^{14}$ m$^{-2}$ as shown in Fig. 3c.

These findings indicate the importance of room temperature-HPT processing of the investigated alloy, where the hot deformation behaviour has improved significantly as observed from the elongation measurements and strain rate sensitivity values.

The morphology of the AM-deposited alloy has been significantly altered after processing in HPT, where the melt pools of the as-deposited alloy fragmented into a finer nm-sized grain structure. The eutectic silicon continuous network has also fragmented into nanosized particles and their distribution increased as the deformation increased. These nanosized particles were aligned with the direction of torsional deformation and finally showed a fairly uniform distribution within the α-Al grains. The refinement in the alloy matrix and eutectic phase is
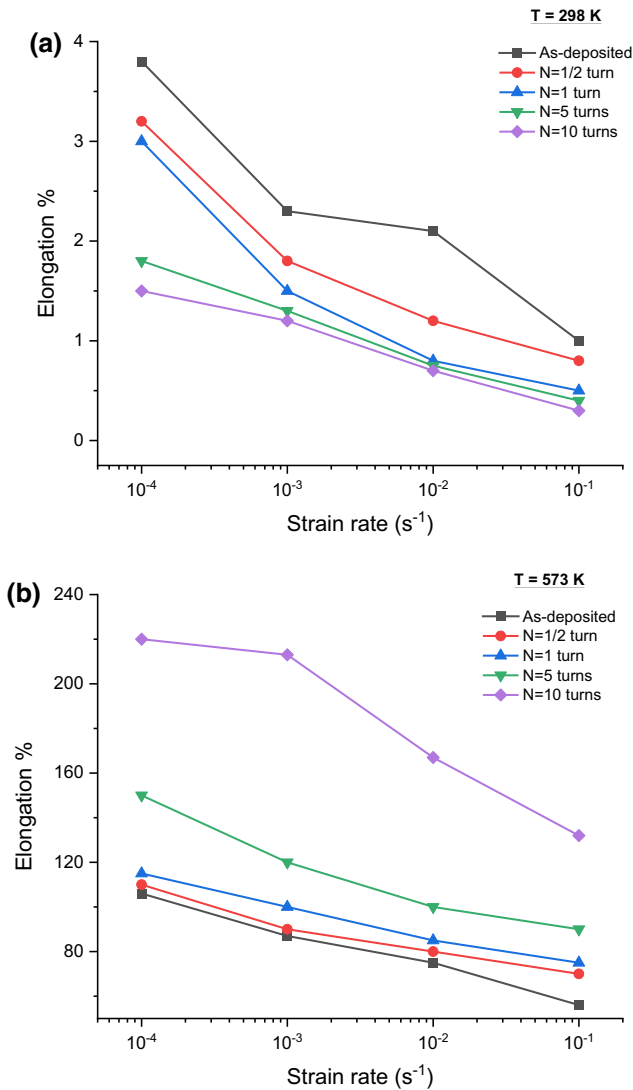
**Figure 8** Elongation-to-fracture for the as-deposited and HPT-processed samples at different rates of tensile strain and at **a** 298 K and **b** 573 K.



**Figure 9** Log–log curve of the variation in the flow stress with strain rate showing the values of strain rate sensitivity for the as-deposited and HPT-processed samples for 10 turns at a testing temperature of 573 K.

attributed directly to the torsional and compressive strains that are imposed during HPT processing, which led to the subdivision of the melt pool into finer structures of nano sizes [7–9, 29–31].

## Mechanical behaviour at room and elevated temperatures

The stress-elongation curves for the as-deposited and HPT-deformed samples that were tested at ambient and elevated testing temperatures revealed that the ultrafine microstructure achieved after HPT has resulted in large elongations at elevated testing temperature compared to results of testing at ambient
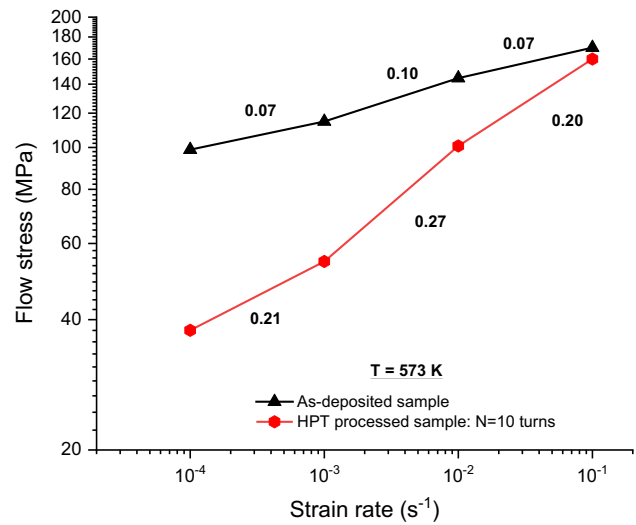
temperature, as shown in Figs. 5 and 6. The maximum elongation for the AM processed alloy was 220% at a strain rate of $10^{-4}$ s$^{-1}$; which (to the authors' knowledge) is the highest elongation achieved for such AM build Al–9%Si–3%Cu alloy.

The current results of elongations to failure were remarkably higher than counterparts reported previously for Al–Si–Cu–Mg alloy [32], where the maximum elongation obtained for the aforementioned alloy was only 12% at a strain rate of $10^{-3}$ s$^{-1}$ and a temperature of 573 K. The present results were also higher than the data reported for Al–Si–Cu–Mg alloy with a maximum elongation of 36% [33] that was obtained using a strain rate of $10^{-4}$ s$^{-1}$ and a temperature of 773 K. The current elongation data were also higher than that reported for Al–11%Si alloy [11] which exhibited an elongation of 34% using a strain rate of $2.3 \times 10^{-3}$ s$^{-1}$ and a temperature of 573 K.

The present elongations were also higher than reported for Al–11%Si alloy with the previously highest reported elongation of 150% at strain rate of $5 \times 10^{-4}$ s$^{-1}$ and at a temperature of 788 K [34]. It is widely reported that Al–Si alloys with ultrafine microstructures can be fabricated at room temperature by severe plastic deformation processes rather than at elevated temperature [9, 35, 36]. Therefore, these fine microstructures would give higher elongations during forming at high temperatures, where the existence of the fine grains is required for

**Figure 10** Surface morphology of the microstructures as seen using SEM on the gauge lengths of as-deposited samples that tested at 573 K and various rates of strain in the tensile test.
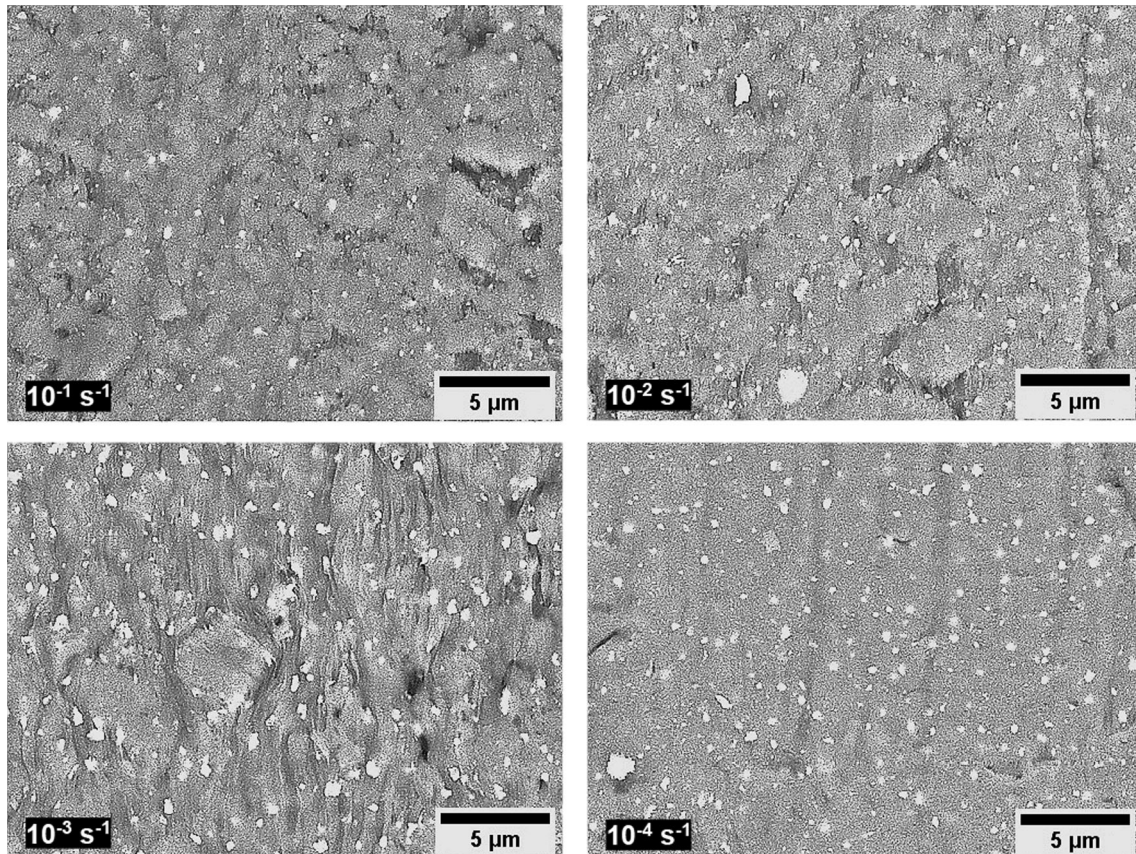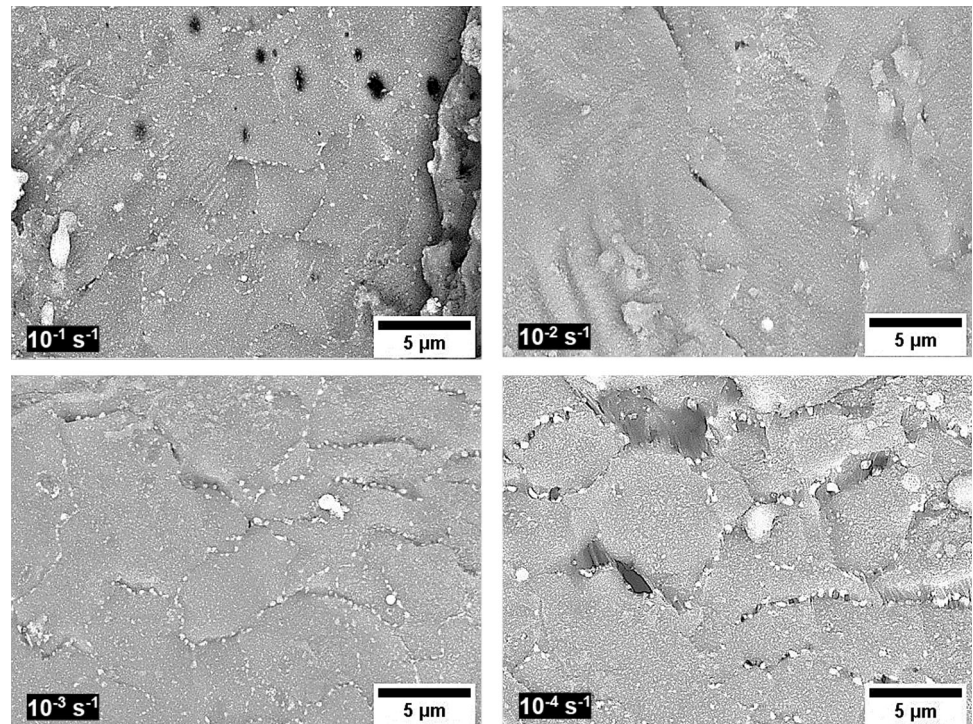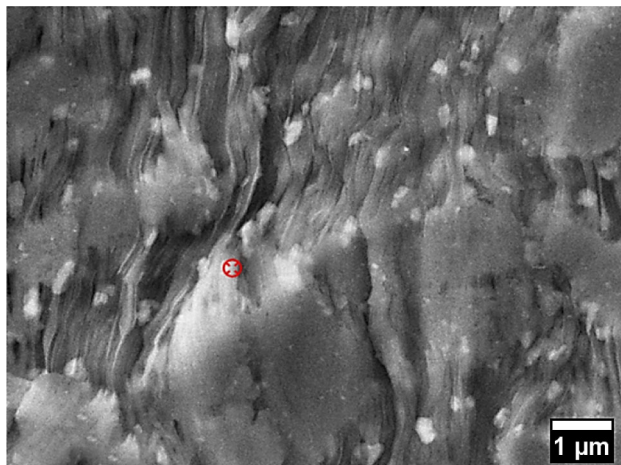




**Figure 11** Surface morphology of the microstructures as seen using SEM on the gauge lengths of HPT-processed samples for 10 turns that tested at 573 K and various rates of strain in the tensile test.

| Element | Weight % |
|---------|----------|
| O | 6.83 |
| Cu | 3.74 |
| Al | 78.36 |
| Si | 11.06 |

**Figure 12** EDS analysis of the elemental fractions on the grain structure of the HPT-processed sample by 10 turns and inspected through the tensile test at 573 K and $10^{-4}$ s$^{-1}$.

achieving superplastic flow in the polycrystalline materials [37–39].

The higher number of HPT turns has led to finer microstructure of AM-deposited Al–9%Si–3%Cu alloy down to 90 nm for the sample deformed using 10 turns. Thus, the elongations at the elevated temperature of testing (573 K) were increased with increasing number of HPT turns at which the samples were processed in HPT compared to the as-deposited samples as shown in Figs. 5 and 6. The elongations of the deformed samples were lower than in the as-deposited samples when tensile testing was conducted at ambient temperature (298 K) due to the increment in the work hardening that is imposed within the processed samples as the deformation increased with a higher number of HPT turns [8–10].

The ambient temperature-hardenability of the HPT-processed samples was assessed using Vickers microhardness measurements of these samples. It was found that the strength (in terms of hardness measurement) of additively manufactured Al–9%Si–3%Cu alloy has increased from 120 to 240HV after 10 HPT turns. This level of strengthening was associated with a substantial density of dislocations up to $6.2 \times 10^{14}$ m$^{-2}$ that contributed mainly to a higher level of strain hardening and lower ductility at ambient temperature-tensile testing for all processed

samples in comparison with the as-deposited samples as exhibited in Figs. 5 and 6.

The elongation increased with a higher number of HPT turns where finer microstructures have been obtained during the HPT as illustrated in Figs. 6, 7 and 8, where the increase in value of the strain rate sensitivity indicates significant resistance to necking failure and allows remarkable elongations to occur [40, 41]. The microstructures after the tensile test remained relatively contiguous, especially at slower strain rates ($10^{-3}$ and $10^{-4}$ s$^{-1}$) as observed along the gauge length regions of the HPT-processed samples after tension as exhibited in Fig. 10, compared to the microstructures of the as-deposited samples at the same strain rate and temperature as seen in Fig. 9.

The migration of grain boundaries during the hot deformation at slower strain rates ($10^{-3}$ and $10^{-4}$ s$^{-1}$) at temperature of 573 K are seen in Figs. 10 and 11, where the discontinuities at grain boundaries would be associated with lower concentration of stresses. Therefore, the deformation mechanisms that govern the deformation at this stage are creep via glide-dislocation associated with the sliding of grain boundaries. The sensitivity values which were close to 0.3 as shown in Fig. 9 confirms this assumption, where the grains remained relatively equiaxed [34, 42].

## Thermal stability of the microstructure

In the current investigation, the AM-deposited Al–9%Si–3%Cu alloy deformed by HPT at room temperature showed an ultrafine grain structure that exhibited significant thermal stability and plasticity at elevated temperature compared to the behaviour of counterpart alloys such as in Al–Si–Cu–Mg [32] Al–Si–Cu-Mg cast alloy [33] Al–11%Si alloy deformed by rotary-die equal channel angular pressing [11, 34]. This may be ascribed to the effects of grain size and particle size and distribution of the eutectic silicon phase. The current as-deposited unprocessed Al–Si–Cu had grainy melt pool structures of average width of 150 µm, whereas the silicon eutectic phase appeared with a continuous network appearance that agglomerated along the melt pool boundaries as seen in Fig. 1a, c.

Following the HPT processing at room temperature, this morphology has changed significantly where an extensive microstructural refinement has been achieved down to average grain size and crystallite size of 90 and 30 nm, respectively. The eutectic

phase has also undergone severe fragmentation into fine particles with an average size of 175 nm with relatively uniform distribution within the alloy matrix with increasing turns of HPT by the virtue of heavily torsional straining during HPT. The fine particles of silicon eutectic phase were distributed homogeneously and appeared as white fine particles as shown in Fig. 2d, for the sample processed in HPT for 10 turns compared to the network morphology of this phase in the as-deposited sample as shown in Fig. 2c.

The existence of eutectic particles with fine sizes and relatively uniform dispersion within the alloy matrix will suppress any rapid grain growth during hot deformation [38, 43]. Therefore, the ultrafine microstructure has better thermal stability compared to their counterparts with larger grain size during the hot deformation due to activation of different mechanisms of superplasticity that precede the grain growth, resulting in remarkable flow and elongations rather than cavitation failure under the hot deformation conditions [37, 38].

The melting point of the silicon eutectic phase in the current alloy is 833 K (560 °C) that is somewhat lower than for the alloy itself (873 K, 600 °C) [1]. Therefore, it is expected that this phase will glide along the grain boundaries at a rate relatively more easily than the grains. The eutectic particles with the lower fraction volume as in the as-deposited alloy were distributed at the grain boundaries and pool boundaries as seen in Fig. 1a, c.

The distribution and volume fraction of eutectic *fine* particles has increased significantly as seen in Fig. 1c, d with additional HPT turns in comparison with their counterparts in the as-deposited unprocessed alloy. The localization of these particles on the aforementioned locations added to a pinning effect, where the dislocations accumulated around these nanoparticles and then strengthening of the samples under tension at a temperature of 298 K [44, 45].

Consequently, the tensile strengths of the additively manufactured Al–9%Si–3%Cu as-deposited and HPT-processed samples at room temperature were significantly better than earlier reports [11, 14, 15], where the maximum tensile strengths have reached 400 and 700 MPa for the as-deposited and processed samples, respectively. These are considerably higher than counterpart reported values after rotary-die ECAP, e.g. Al–11%Si alloy with

250 MPa [11], ECAP-Al–10%Si alloy with 234 MPa [14], and ECAP-Al–7%Si alloy with 250 MPa [15].

This confirms the uniformity of tensile deformation at room temperature was maintained and assisted by the relatively homogeneous distribution of fine particles of silicon eutectic phase after HPT processing compared to ECAP processing [44]. The considerably higher values of the tensile strengths of as-deposited samples and processed samples when tested at 298 K compared to reports in [11, 14, 15], make the combination of HPT processing with additively manufactured Al–Si alloy potentially highly desirable in designing novel alloy processing routes for appropriate industrial applications.

Another factor that plays a significant part in the strengthening of as-deposited samples is the effect of microstructure morphology with regard to the tensile loading direction. The current alloy was built vertically, i.e. along the z-axis that represents the alloy rod length as schematically shown in [46], then the HPT disc was cut parallel to the x–y plane which is the same orientation as the tensile samples. The elongated grain morphology in terms of melt pool shapes was parallel to the tensile loading, which results in considerably enhanced tensile strength.

The deformation continuity was maintained via melt pools that lie parallel to the loading direction until it reached a point at which the hardening capability was increased by the cross-linking of these pools of different directions. Eventually, cavitation appeared in the as-deposited samples due to the coalescence of lack-of-fusion and gas micropores leading to the failure at relatively lower elongations during tensile testing at room temperature compared to conventional Al–Si alloys [16].

The nanosized particles enhanced the sliding of grains significantly at a temperature of 573 K for the HPT-deformed samples compared to the as-deposited samples. It has been suggested that the second phase particles act as a lubrication of the grains sliding under hot deformation conditions [47, 48], where the testing temperature of 573 K corresponds $0.68\ T_m$ of the silicon eutectic phase that is relatively higher than for the matrix alloy of $0.65\ T_m$ [1]. Hence, the higher elongations achieved for deformed samples by 10 turns in HPT compared to the elongations in the as-deposited samples, were assisted by the high-volume fraction of the fine particles of eutectic silicon phase as seen in Figs. 3, 4 and 5 [11, 49].

Filaments or fibrous structures appeared at lower strain rates and elevated temperature of 573 K for the processed samples rather than the as-deposited samples as observed in Figs. 11 and 12. These structures were aligned parallel to the tension direction and their role is reconnecting the disconnected grains and grain boundaries, as well as relinking the surface cavities that appear at the final stage of hot deformation. Therefore it seems that the higher values of elongations and alloy flow under conditions of elevated testing temperature and slower strain rate were maintained by the formation of the fibrous structures as observed in Fig. 10 [47, 48, 50].

The chemical composition of the fibrous structures was analysed using EDS as shown in Fig. 12, which confirmed that these structures are mainly composed of α-Al matrix grains, as indicated by the weight fractions of elements in the sample processed for 10 turns in HPT and then tested in tension using a strain rate of $10^{-4}$ s$^{-1}$ at testing temperature of 573 K with an achieved elongation of 220%. It is worth noting that all samples have been exposed to oxidation as revealed by the oxygen weight ratio in the EDS data that presented in Fig. 12, as all tensile tests were carried out in air.

Fibrous structures were not observed in the as-deposited tensile samples as shown in Fig. 10, that were tested at a temperature of 573 K at all rates of strain. Instead, a cavitation failure was observed at slower strain rates of $10^{-3}$ and $10^{-4}$ s$^{-1}$ as seen in Fig. 10. This can be attributed to effects of the larger grain size and particle size and distribution of the eutectic phase in these as-deposited samples.

In the aforementioned conditions of tensile testing, grain growth is expected, where the measured grain size after high temperature testing was about 10 μm in the as-deposited tensile samples compared to the grain size of 5 μm in the tensile samples that were processed earlier for 10 HPT turns. The grain growth in the processed tensile samples was relatively inhibited by the existence of ultrafine grains and nanosized well-distributed eutectic particles [38, 43].

The ultrafine grains are believed to preferably undergo glide-dislocation creep and slide over each other as indicated by the measurement of strain rate sensitivity. The distribution of nanosized eutectic particles within the α-Al grains and along the grain boundaries resulted in relative retardation of cavitation and assisted grain sliding due to the softening of this phase at elevated testing temperature [11, 43].

The non-spherical morphology of the eutectic phase for as-deposited samples, compared to the relatively spherical morphology of the nanosized eutectic particles in the processed samples, operate as sites for crack initiation leading to a reduction in the elongation to failure of as-deposited samples compared to that found in the processed samples at the same conditions of strain rates and testing temperature [4, 16].

## Conclusions

1. Effective HPT processing at room temperature produced an extensive microstructural refinement to about 90 nm with high estimated value of dislocations of $6.2 \times 10^{14}$ m$^{-2}$, that considerably improves the ambient temperature-hardness of the additively manufactured alloy from 120 to 240 HV.

2. The as-deposited and processed samples exhibited significant tensile strengths of 400 and 700 MPa, respectively, that are remarkably higher compared to the cast counterpart alloys.

3. Excellent elongation values were achieved for the AM-deposited alloy up to 106% and 220% at 573 K for the as-deposited and processed samples, respectively, that are considerably higher than the cast counterpart alloys reported in the literature.

4. The ultrafine α-Al and nanosized eutectic Si particles produced by HPT have improved the microstructural stability of the processed samples compared to as-deposited samples at all rates of tensile strain and at elevated temperature of 573 K.

5. Formation of fibrous structures has improved the flow, elongation, and cavitation resistance of the processed samples at elevated testing temperature and slow strain rates.

## Author contribution

ASJA-Z contributed to methodology, investigation, formal analysis, and writing–initial draft. PASR and NG performed supervision, conceptualization, and writing–review and editing. JD performed tensile tests and editing, PP performed SEM and EDS observations. SS and DK carried out TEM sample preparation and observations. YC performed STEM and EDS observations.

## Declarations

**Conflict of interest**   The authors state that they have no competitive financial interests or known personal links that would have affected the research presented here.

**Supplementary Information:** The online version contains supplementary material available at https://doi.org/10.1007/s10853-022-07847-9.

## References

[1] Ye H (2003) An overview of the development of Al–Si-alloy based material for engine applications. J Mater Eng Perform 12:288–297. https://doi.org/10.1361/105994903770343132

[2] Hernandez FCR, Ramírez JMH, Mackay R (2017) Al–Si alloys: automotive, aeronautical, and aerospace applications. Springer, Cham. https://doi.org/10.1007/978-3-319-58380-8

[3] Tavitas-Medrano FJ, Gruzleski JE, Samuel FH, Valtierra S, Doty HW (2008) Effect of Mg and Sr-modification on the mechanical properties of 319-type aluminum cast alloys subjected to artificial aging. Mater Sci Eng A 480:356–364. https://doi.org/10.1016/j.msea.2007.09.002

[4] Li XP, Wang XJ, Saunders M, Suvorova A, Zhang LC, Liu YJ, Fang MH, Huang ZH, Sercombe TB (2015) A selective laser melting and solution heat treatment refined Al–12Si alloy with a controllable ultrafine eutectic microstructure and 25% tensile ductility. Acta Mater 95:74–82. https://doi.org/10.1016/j.actamat.2015.05.017

[5] Hegde S, Prabhu KN (2008) Modification of eutectic silicon in Al–Si alloys. J Mater Sci 43:3009–3027. https://doi.org/10.1007/s10853-008-2505-5

[6] Jiang B, Ji Z, Hu M, Xu H, Xu S (2019) A novel modifier on eutectic Si and mechanical properties of Al–Si alloy. Mater Lett 239:13–16. https://doi.org/10.1016/j.matlet.2018.12.045

[7] Zhao LZ, Zhao MJ, Song LJ, Mazumder J (2014) Ultra-fine Al–Si hypereutectic alloy fabricated by direct metal deposition. Mater Des 56:542–548. https://doi.org/10.1016/j.matdes.2013.11.059

[8] Mungole T, Nadammal N, Dawra K, Kumar P, Kawasaki M, Langdon TG (2013) Evolution of microhardness and microstructure in a cast Al–7 % Si alloy during high-pressure torsion. J Mater Sci 48:4671–4680. https://doi.org/10.1007/s10853-012-7061-3

[9] El Aal MIA, Kim HS (2014) Wear properties of high pressure torsion processed ultrafine grained Al–7%Si alloy. Mater Des 53:373–382. https://doi.org/10.1016/j.matdes.2013.07.045

[10] Wang X, Nie M, Wang CT, Wang SC, Gao N (2015) Microhardness and corrosion properties of hypoeutectic Al–7Si alloy processed by high-pressure torsion. Mater Des 83:193–202. https://doi.org/10.1016/j.matdes.2015.06.018

[11] Ma A, Takagi M, Saito N, Iwata H, Nishida Y, Suzuki K, Shigematsu I (2005) Tensile properties of an Al–11mass%Si alloy at elevated temperatures processed by rotary-die equal-channel angular pressing. Mater Sci Eng A 408:147–153. https://doi.org/10.1016/j.msea.2005.07.064

[12] Aboulkhair NT, Maskery I, Tuck C, Ashcroft I, Everitt NM (2016) The microstructure and mechanical properties of selectively laser melted AlSi10Mg: the effect of a

conventional T6-like heat treatment. Mater Sci Eng A 667:139–146. https://doi.org/10.1016/j.msea.2016.04.092

[13] Lowe TC, Valiev RZ (2004) The use of severe plastic deformation techniques in grain refinement. Jom 56:64–68. https://doi.org/10.1007/s11837-004-0295-z

[14] Regina Cardoso K, Muñoz-Morris MA, Valdés León K, Morris DG (2013) Room and high temperature ECAP processing of Al–10%Si alloy. Mater Sci Eng A 587:387–396. https://doi.org/10.1016/j.msea.2013.09.006

[15] Natori K, Utsunomiya H, Tanaka T (2017) Improvement in formability of semi-solid cast hypoeutectic Al–Si alloys by equal-channel angular pressing. J Mater Process Technol 240:240–248. https://doi.org/10.1016/j.jmatprotec.2016.09.022

[16] Aboulkhair NT, Simonelli M, Parry L, Ashcroft I, Tuck C, Hague R (2019) 3D printing of Aluminium alloys: additive manufacturing of aluminium alloys using selective laser melting. Prog Mater Sci 106:100578. https://doi.org/10.1016/j.pmatsci.2019.100578

[17] Prashanth KG, Scudino S, Eckert J (2017) Defining the tensile properties of Al–12Si parts produced by selective laser melting. Acta Mater 126:25–35. https://doi.org/10.1016/j.actamat.2016.12.044

[18] Mohd Yusuf S, Chen Y, Yang S, Gao N (2020) Microstructural evolution and strengthening of selective laser melted 316L stainless steel processed by high-pressure torsion. Mater Charact 159:110012–110024. https://doi.org/10.1016/j.matchar.2019.110012

[19] Al-Zubaydi ASJ, Zhilyaev AP, Wang SC, Kucita P, Reed PAS (2016) Evolution of microstructure in AZ91 alloy processed by high-pressure torsion. J Mater Sci 51:3380–3389. https://doi.org/10.1007/s10853-015-9652-2

[20] Gubicza J, El-Tahawy M, Lábár JL, Bobruk EV, Murashkin MY, Valiev RZ, Chinh NQ (2020) Evolution of microstructure and hardness during artificial aging of an ultrafine-grained Al–Zn–Mg–Zr alloy processed by high pressure torsion. J Mater Sci 55:16791–16805. https://doi.org/10.1007/s10853-020-05264-4

[21] Xu C, Horita Z, Langdon TG (2007) The evolution of homogeneity in processing by high-pressure torsion. Acta Mater 55:203–212. https://doi.org/10.1016/j.actamat.2006.07.029

[22] Voort V, Baldwin W (2004) Metallography and microstructures handbook. ASM Int 9:2733

[23] Sakai G, Horita Z, Langdon TG (2005) Grain refinement and superplasticity in an aluminum alloy processed by high-pressure torsion. Mater Sci Eng A 393:344–351. https://doi.org/10.1016/j.msea.2004.11.007

[24] Harai Y, Kai M, Kaneko K, Horita Z, Langdon TG (2008) Microstructural and mechanical characteristics of AZ61 magnesium alloy processed by high-pressure torsion. Mater Trans 49:76–83. https://doi.org/10.2320/matertrans.ME200718

[25] Melzer D, Smirnov I, Lukáš O, Dlouhý J, Evstifeev A, Džugan J, Valiev R (2022) Fracture locus characteristics of Al alloy 5083 processed by equal channel angular pressing using miniaturized specimens. J Alloys Compd 889:161675–161687. https://doi.org/10.1016/j.jallcom.2021.161675

[26] Máthis K, Köver M, Stráská J, Trojanová Z, Džugan J, Halmešová K (2018) Micro-tensile behavior of Mg–Al–Zn alloy processed by equal channel angular pressing (ECAP). Materials (Basel) 11:1644–1655. https://doi.org/10.3390/ma11091644

[27] Džugan J, Procházka R, Konopík P (2015) Micro-tensile test technique development and application to mechanical property determination. In: ASTM Special Technical Publication, pp 12–30. https://doi.org/10.1520/STP157620140022.

[28] Gubicza J (2015) Correlation between processing conditions, lattice defect structure and mechanical performance of ultrafine-grained materials. Acta Phys Pol A 128:479–485. https://doi.org/10.12693/APhysPolA.128.479

[29] Zhao W, Han J-K, Kuzminova YO, Evlashin SA, Zhilyaev AP, Pesin AM, Jang J, Liss K-D, Kawasaki M (2021) Significance of grain refinement on micro-mechanical properties and structures of additively-manufactured CoCrFeNi high-entropy alloy. Mater Sci Eng A 807:140898. https://doi.org/10.1016/j.msea.2021.140898

[30] Lee HJ, Han JK, Janakiraman S, Ahn B, Kawasaki M, Langdon TG (2016) Significance of grain refinement on microstructure and mechanical properties of an Al–3%Mg alloy processed by high-pressure torsion. J Alloys Compd 686:998–1007. https://doi.org/10.1016/j.jallcom.2016.06.194

[31] Al-Zubaydi ASJ, Gao N, Wang S, Reed PAS (2022) Microstructural and hardness evolution of additively manufactured Al–Si–Cu alloy processed by high-pressure torsion. J Mater Sci 57:8956–8977. https://doi.org/10.1007/s10853-022-07234-4

[32] Shaha SK, Czerwinski F, Kasprzak W, Friedman J, Chen DL (2016) Ageing characteristics and high-temperature tensile properties of Al–Si–Cu–Mg alloys with micro-additions of Cr, Ti, V and Zr. Mater Sci Eng A 652:353–364. https://doi.org/10.1016/j.msea.2015.11.049

[33] Zamani M, Seifeddine S, Jarfors AEW (2015) High temperature tensile deformation behavior and failure mechanisms of an Al–Si–Cu–Mg cast alloy–the microstructural scale effect. Mater Des 86:361–370. https://doi.org/10.1016/j.matdes.2015.07.084

[34] Jing-hua J, Ai-bin M, Saito N, Watazu A, Ping-hua L, Nishida Y (2007) Effect of microstructures on superplasticity of Al–11%Si alloy. Trans Nonferrous Metals Soc China 17:509–513

[35] Zhilyaev AP, García-Infanta JM, Carreño F, Langdon TG, Ruano OA (2007) Particle and grain growth in an Al–Si alloy during high-pressure torsion. Scr Mater 57:763–765. https://doi.org/10.1016/j.scriptamat.2007.06.029

[36] Jiang J-H, Ma A-B, Lu F-M, Saito N, Watazu A, Song D, Zhang P, Nishida Y (2011) Improving corrosion resistance of Al–11mass%Si alloy through a large number of ECAP passes. Mater Corros 62:848–852. https://doi.org/10.1002/maco.200905521

[37] Davies GJ, Edington JW, Cutler CP, Padmanabhan KA (1970) Superplasticity: a review. J Mater Sci 5:1091–1102. https://doi.org/10.1007/BF02403283

[38] Kawasaki M, Langdon TG (2015) Review: achieving superplastic properties in ultrafine-grained materials at high temperatures. J Mater Sci 51:19–32. https://doi.org/10.1007/s10853-015-9176-9

[39] Kawasaki M, Il Jang J, Langdon TG (2018) Superplastic flow and micro-mechanical response of ultrafine-grained materials. Defect Diffus Forum 385:9–14. https://doi.org/10.4028/www.scientific.net/DDF.385.9

[40] Langdon TG (1994) A unified approach to grain boundary sliding in creep and superplasticity. Acta Metall Mater 42:2437–2443. https://doi.org/10.1016/0956-7151(94)90322-0

[41] Raghavan KS (1984) Superplasticity. Bull Mater Sci 6:689–698

[42] Nieh T-G, Wadsworth J, Sherby OD (2005) Superplasticity in metals and ceramics. Cambridge University Press, Cambridge

[43] Nakayama Y, Miyazaki T (2011) Effect of eutectic si particle morphology on ECAP formability and mechanical properties of AC4CH aluminum casting alloys. Mater Trans 52:2045–2051. https://doi.org/10.2320/matertrans.L-M2011822

[44] Zhang X, Huang LK, Zhang B, Chen YZ, Liu F (2020) Microstructural evolution and strengthening mechanism of an Al–Si–Mg alloy processed by high-pressure torsion with different heat treatments. Mater Sci Eng A 794:139932–139944. https://doi.org/10.1016/j.msea.2020.139932

[45] Zhang X, Huang LK, Zhang B, Chen YZ, Duan SY, Liu G, Yang CL, Liu F (2019) Enhanced strength and ductility of A356 alloy due to composite effect of near-rapid solidification and thermo-mechanical treatment. Mater Sci Eng A 753:168–178. https://doi.org/10.1016/j.msea.2019.03.039

[46] Yusuf SM, Hoegden M, Gao N (2020) Effect of sample orientation on the microstructure and microhardness of additively manufactured AlSi10Mg processed by high-pressure torsion. Int J Adv Manuf Technol 106:4321–4337. https://doi.org/10.1007/s00170-019-04817-5

[47] Lee SW, Chen YL, Wang HY, Yang CF, Yeh JW (2007) On mechanical properties and superplasticity of Mg–15Al–1Zn alloys processed by reciprocating extrusion. Mater Sci Eng A 464:76–84. https://doi.org/10.1016/j.msea.2007.01.119

[48] Al-Zubaydi ASJ, Zhilyaev AP, Wang SC, Reed PAS (2015) Superplastic behaviour of AZ91 magnesium alloy processed by high-pressure torsion. Mater Sci Eng A 637:1–11. https://doi.org/10.1016/j.msea.2015.04.004

[49] Tutunchilar S, Besharati Givi MK, Haghpanahi M, Asadi P (2012) Eutectic Al–Si piston alloy surface transformed to modified hypereutectic alloy via FSP. Mater Sci Eng A 534:557–567. https://doi.org/10.1016/j.msea.2011.12.008

[50] Pojda VP, Bryukhovetskii VV, Poida AV, Kuznetsova RI, Klepikov VF, Voronov DL (2007) Morphology and mechanisms of the formation of fiber structures upon high-temperature superplastic deformation of aluminum alloys. Phys Metals Metallogr 103:414–423. https://doi.org/10.1134/S0031918X07040151